

H -dibaryon and hypernucleus formation in the $\Xi^{-12}\text{C}$ reaction at rest

J. K. Ahn,^{1,*} S. Aoki,⁴ K. S. Chung,¹¹ M. S. Chung,¹⁰ H. En'yo,¹ T. Fukuda,⁵ H. Funahashi,¹ Y. Goto,^{1,†} A. Higashi,⁵ M. Ieiri,⁶ T. Iijima,⁶ M. Iinuma,¹ K. Imai,¹ Y. Itow,^{1,‡} J. M. Lee,¹¹ S. Makino,¹ A. Masaïke,¹ Y. Matsuda,¹ Y. Matsuyama,⁵ S. Mihara,¹ C. Nagoshi,⁵ I. Nomura,⁸ I. S. Park,¹⁰ N. Saito,^{1,†} M. Sekimoto,⁵ Y. M. Shin,⁹ K. S. Sim,¹⁰ R. Susukita,^{1,†} R. Takashima,² F. Takeuchi,³ P. Tlustý,^{5,§} S. Weibe,⁹ S. Yokkaichi,¹ K. Yoshida,¹ M. Yoshida,^{1,†} T. Yoshida,⁷ and S. Yamashita^{1,||}

(KEK-PS E224 Collaboration)

¹Department of Physics, Kyoto University, Kyoto 606-8502, Japan²Kyoto University of Education, Kyoto 612, Japan³Kyoto Sangyo University, Kyoto 606, Japan⁴Faculty of Human Development, Kobe University, Kobe 657-8501, Japan⁵Institute for Nuclear Study, University of Tokyo, Tokyo 188-8501, Japan⁶KEK, High Energy Accelerator Research Organization, Tsukuba 305, Japan⁷Department of Physics, Osaka City University, Osaka 558-8585, Japan⁸National Institute for Fusion Science, Nagoya 464, Japan⁹University of Saskatchewan, Saskatoon, Canada¹⁰Department of Physics, Korea University, Seoul 136-701, Korea¹¹Department of Physics, Yonsei University, Seoul 120-749, Korea

(Received 23 March 2000; published 2 October 2000)

Stopped- $\Xi^{-12}\text{C}$ reactions have been investigated with respect to H -dibaryon and hypernucleus formation with a scintillating fiber detector. Out of 5.5×10^3 tagged Ξ^{-} particles via the (K^{-}, K^{+}) reaction we obtained 72 stopping Ξ^{-} events with $6.7_{-1.4}^{+1.1}$ background events after imposing kinematic constraints. Hypernuclear production has been studied by observing free Λ decays in the stopped- Ξ^{-} reactions. From the observed Λ momentum spectrum, we have found the hypernuclear production rates to be 18 ± 13 , 65 ± 6 , and 17 ± 12 % for double/twin- Λ hypernucleus, single- Λ hypernucleus, and no hypernucleus cases, respectively. With the same sample, we set upper limits on R (stopped- $\Xi^{-12}\text{C} \rightarrow HX$ / stopped- $\Xi^{-12}\text{C} \rightarrow$ all) for H decaying into Λn , $\Sigma^{-}p$, and $\Lambda p \pi^{-}$, for H masses just below $\Lambda\Lambda$ mass threshold and for H lifetime range $10^{-11} \leq \tau_H \leq 10^{-8}$ s. The upper limits on R are ~ 0.1 – 0.2 , assuming all of the H decay into each decay mode. Our results give a tight constraint on the existence of the bound H , in comparison with the theoretical estimates of Aerts and Dover, albeit with different target nuclei.

PACS number(s): 14.20.Pt, 21.80.+a, 25.80.Pw

I. INTRODUCTION

Double-strangeness ($S = -2$) systems have attracted much attention over several decades, since the question of their properties is of fundamental importance in a field intersecting with nuclear and particle physics. Among them, the lightest $S = -2$ system beyond Ξ hyperons is a possibly bound H -dibaryon, which has a $uuddss$ quark configuration of maximal spatial symmetry [1]. The MIT bag model predicts the mass of the H dibaryon, for the S -wave flavor singlet with $J^{\pi} = 0^{+}$, to be $m_H = 2.150 \text{ GeV}/c^2$. For the mass

interval between Λn ($2.055 \text{ GeV}/c^2$) and $\Lambda\Lambda$ ($2.231 \text{ GeV}/c^2$) thresholds the H particle would decay predominantly by nonleptonic weak decay into two baryons in $\Delta S = 1$ transitions. The more conventional nonleptonic decay involving pions $H \rightarrow \Lambda N \pi$ is allowed if $m_H > 2.194 \text{ GeV}/c^2$ [2].

Despite strenuous experimental efforts using a variety of approaches, there has been as yet no definitive observation of such a deeply bound (by more than 30–50 MeV) H -dibaryon [3]. Instead, the observation of several double- Λ hypernuclear events in nuclear emulsion suggests that the H -dibaryon is very loosely bound, or unbound, relative to $2m_{\Lambda}$ [4]. While experimental searches for an unbound H dibaryon yielded no conclusive evidence in high-energy experiments [5–7], we observed in our previous analysis enhanced $\Lambda\Lambda$ production near the threshold in $^{12}\text{C}(K^{-}, K^{+})$ reaction [8]. It is suggestive of either the possible existence of a $\Lambda\Lambda$ resonance (as an H -dibaryon resonance), a strongly attractive $\Lambda\Lambda$ final state interaction, or both.

An alternative scheme for H production is the formation from Ξ^{-} atoms via the $\Xi^{-}p$ fusion processes, first suggested by Barnes [9]. Quantitative predictions for the branching ratio for H formation from various states of $\Xi^{-}p$, $\Xi^{-}d$,

*Present address: RCNP, Research Center for Nuclear Physics, Osaka University, Osaka 567-0047, Japan.

†Present address: RIKEN, Institute for Physical and Chemical Research, Wako 351-0198, Japan.

‡Present address: Institute for Cosmic Ray Research, University of Tokyo, Tokyo 188-8502, Japan.

§Present address: Nuclear Physics Institute of the Academy of Science, 250 68 Reř, Āzech Republic.

||Present address: International Center for Elementary Particle Physics, University of Tokyo, Tokyo 113, Japan.

and $\Xi^{-4}\text{He}$ atoms were given by Aerts and Dover [10]. These initiated the H -search experiment E813 at BNL using a deuterium target and tagged Ξ^{-} via the (K^{-}, K^{+}) reaction [3]. The theoretical estimates show that branching ratios for H production from $\Xi^{-}d$ atom approaches 0.9 for S states in Nijmegen model D , for m_H near the $\Lambda\Lambda$ threshold, but no larger than 0.25 in model F . The branching ratios for P states are even smaller than those for S states. The case of the $\Xi^{-4}\text{He}$ atom is, however, predicted in both model D and model F to yield quite large values for the branching ratio, approaching 1.0 near $\Lambda\Lambda$ threshold. Although our results cannot be compared directly with the estimates of Aerts and Dover [10] due to different target nuclei, it should be noted that our experimental approach is sensitive enough to give a meaningful constraint on the existence of the bound H in the region near the $\Lambda\Lambda$ threshold.

Single event evidence for the existence of double- Λ hypernuclei, ${}_{\Lambda\Lambda}^{10}\text{Be}$ [11] and ${}_{\Lambda\Lambda}^6\text{He}$ [12], was reported in early emulsion experiments and more recently in a KEK hybrid-emulsion experiment [4]. The KEK event is kinematically consistent with the formation of either ${}_{\Lambda\Lambda}^{10}\text{Be}$ or ${}_{\Lambda\Lambda}^{13}\text{B}$. The KEK experiment used tagged Ξ^{-} particles from the (K^{-}, K^{+}) reaction. The latter one was the interpretation by Dover *et al.* [13], assuming a relatively long-lived excited state, ${}_{\Lambda\Lambda}^{14}\text{C}^*$, decaying into ${}_{\Lambda\Lambda}^{13}\text{B}+p$.

If one follows the interpretation of Dover *et al.* [13] for the KEK double- Λ hypernuclear event, the binding energy of the two Λ 's for the three observed $\Lambda\Lambda$ hypernuclei is approximately 4–5 MeV. This result implies that the 1S_0 ΛN interaction is more attractive than the 1S_0 ΛN (2–3 MeV) and comparable to the 1S_0 NN interaction (5–8 MeV). However, it does not give a direct answer to the intriguing question: *is* the two-body 1S_0 $\Lambda\Lambda$ system a quasinuclear (weakly bound) state or an unbound state analogous to the 1S_0 nn system? This is because a fully microscopic, realistic $8N+2\Lambda$ calculation of ${}_{\Lambda\Lambda}^{10}\text{Be}$, for example, is not practical, and the answer is quite model dependent.

Fragmentation of the $S=-2$ system due to a Ξ^{-} -nuclear reaction at rest is of great interest in its own right, since one can explore the production mechanism of double-, twin-, and single- Λ hypernuclei. A quasideuteron model [14] predicts that the reaction $\Xi^{-}d \rightarrow \Lambda\Lambda n$ is responsible for double- Λ hypernucleus formation. Sano *et al.* [15] modeled a compound double- Λ hypernucleus, while Yamada *et al.* [16] suggested doorway states as an intermediate state, ${}_{\Lambda\Lambda}^{13}\text{B}^*$, in which $\Xi^{-}p$ annihilates to $\Lambda\Lambda$ in a nucleus. More recently, Hirata *et al.* [17] calculated formation probabilities of double-, twin-, and single- Λ hypernuclei based on a microscopic transport model [antisymmetrized molecular dynamics (AMD) plus quantal Langevin (QL) method].

A recent experiment, E885 at BNL, reported upper limits on the branching ratio for $(\Xi^{-}, {}^{12}\text{C})_{\text{atom}} \rightarrow {}_{\Lambda\Lambda}^{12}\text{B}+n$ at or below 4% in the region of expected neutron energies [18]. They observed no apparent peaks from the neutron-emission channel of double- Λ hypernuclear formation from $(\Xi^{-}, {}^{12}\text{C})_{\text{atom}}$ decay. The theoretical predictions could also be tested by observing Λ hyperons in the stopped- $\Xi^{-}{}^{12}\text{C}$ reaction. It is worth stressing that the total yield of Λ par-

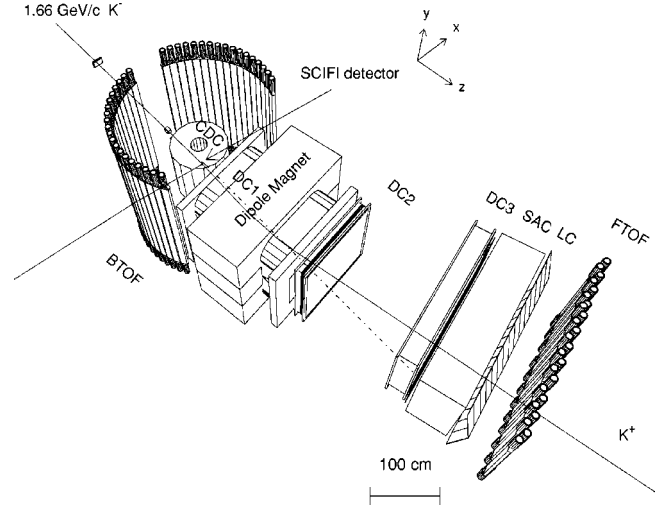


FIG. 1. Layout of the E224 experimental setup shown in a perspective view with a simulated (K^{-}, K^{+}) reaction event.

ticles could answer the question about the formation probabilities of double- and single- Λ hypernuclei, as well as some specific two-body decay channels with single- Λ emission. Our experiment is well suited to observe double- and single- Λ hypernucleus production reactions with stopped- Ξ^{-} events tagged by reconstructing the ${}^{12}\text{C}(K^{-}, K^{+}\Xi^{-})X$ reactions in a scintillating fiber active target.

In this paper, we report on hypernuclear formation probabilities through the Ξ^{-} atomic capture process in ${}^{12}\text{C}$ nuclei, and an upper limit for H -dibaryon production with subsequent weak $\Lambda n, \Sigma^{-}p$, and $\Lambda p \pi^{-}$ decays.

II. EXPERIMENT

The experiment was carried out using a separated 1.66-GeV/c K^{-} beam at the KEK proton synchrotron. The K^{-}/π^{-} ratio of the beam was typically 1/4 at a rate of $2 \times 10^4 K^{-}/\text{spill}$ (~ 2 s). Approximately $8 \times 10^9 K^{-}$ were incident during the experiment. The π^{-}/\bar{p} beam contamination was reduced to 0.1% using the beam line time-of-flight counters and the pulse height from an aerogel Čerenkov counter. The momenta of outgoing particles were measured with a K^{+} spectrometer of approximately 5 m in length, consisting of a dipole analyzing magnet with a field integral of 1.08 Tm, 12 drift-chamber planes (DC1–3), two Čerenkov counters (SAC and LC), and three hodoscope counters for timing and triggering purposes, as shown in Fig. 1. The geometrical acceptance of the spectrometer was about 0.09 sr for 1.1 GeV/c particles. The momentum resolution ($\Delta p/p$) was 0.5% (rms) at 1.2 GeV/c, and the background ratio of π^{+} to K^{+} was estimated to be less than 0.2% [19].

The heart of the experiment is a novel 4π detector consisting of $0.5 \times 0.5\text{-mm}^2$ plastic scintillating fibers. The scintillating fiber (SCIFI) detector acts as a primary interaction target and visual track detector for recognizing (K^{-}, K^{+}) reactions and secondary interactions of hyperons produced in the effective volume of $8 \times 8 \times 10\text{ cm}^3$. About 200 flat sheets, each consisting of 160 plastic scintillating fibers, constituted the SCIFI target. The fiber (SCSF-81) consisted of a

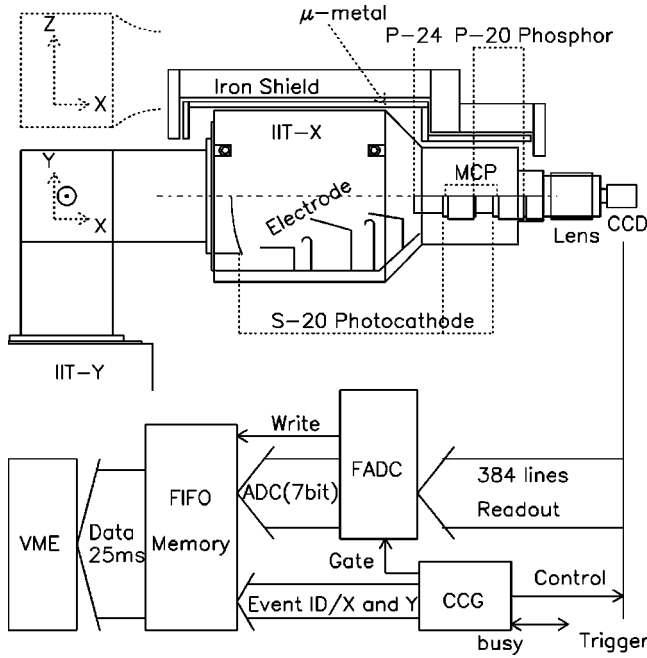


FIG. 2. Sketch of the SCIFI target system and the readout system.

480- μm -thick polystyrene core ($\rho = 1.06 \text{ g/cm}^2$), the exterior of which is covered with a 10 $\mu\text{m}(t)$ cladding layer ($\rho = 1.18 \text{ g/cm}^2$) of polymethylmethacrylate (PMMA). The SCIFI target contained almost equal numbers of carbon and hydrogen atoms. The SCIFI target was observed using two sets of the image-intensifier tubes (IIT), which were arranged orthogonally along the X and Y directions, as shown in Fig. 2. The beam corresponds to the Z direction. The intensified image was recorded using a charge-coupled device (CCD) camera and digitized with a flash analog-to-digital converter (ADC). The SCIFI target was surrounded by a cylindrical drift chamber (CDC) and time of flight (TOF) counters (BTOF) to detect particles coming out of the SCIFI target [20].

The three-stage IIT (Delft PP0040) consisted of an electrostatically focused tube and two proximity-focused micro-channel plate (MCP) tubes. Each IIT stage achieves image conversion between the photocathode and the phosphor screen. The effective photosensitive area of the first stage was 80 mm in diameter and was reduced to 16 mm in diameter at the output. The second and third stages had a one-to-one reduction factor. The IIT's were coupled to the CCD cameras by relay lenses, whose reduction factor was 16 to 6.6. Due to the read-out frequency of the CCD (30 Hz), a fast and efficient method was needed to reduce the trigger rate to a manageable level, about 20 events/spill. To accomplish this, the trigger system was divided into two stages. The first-level trigger selected a positively charged particles in 300 ns. Its signal gated the second-stage IIT's during the 2.5- μs time interval characterizing the decay of the phosphor (P-24) of the first stage IIT's ($\tau_{1/10} = 2.4 \mu\text{s}$). The second-level trigger was made with fast electronics to calculate the masses of the scattered particles within a time of 15 μs . This time limit was due to the 50- μs decay time of the

phosphor of the second stage IIT's. This second-level trigger signal was applied to the last stage IIT's.

The standard NTSC video signals from the CCD chip are digitized by an image digitizer consisting of a clock/coordinate generator (CCG), a parallel flash ADC (FADC) and a "first-in/first-out" (FI/FO) memory buffer. The CCG initiates the DAQ sequence in coincidence with the second level trigger, and generates a common clock to synchronize the CCD and the FADC. The CCD busy signal from the CCG gates the CCD readout sequence until the CCD reads out a first (odd or even) field and transfers the charges stored in the pixels of second field lines into shift registers. The CCD is interrupted during the readout sequence, so as to prevent any piling up of subsequent images on one another. Therefore the width of the gate signal determines the dead time of the CCD readout sequence, which is $\sim 25 \text{ ms}$ on average.

Finally, the data contained in the FI/FO memories are sent via fast transmission lines towards the parallel I/O registers of VME where online SCIFI track information can be provided within $\sim 30 \text{ ms}$. The total dead time during the online data taking was 20%. The SCIFI image data were written on 8-mm magnetic tapes via two sets of the VME dedicated to two CCD signals from horizontal and vertical IIT arms. The data stored in two different tapes were merged during offline data reduction into one data summary tape together with the spectrometer data.

The average number of track clusters for a minimum-ionizing particle was approximately 0.55/mm along the particle track, and the size of a single cluster was typically 180 μm (rms). The track residual, defined as the distribution of the distance between the fitted straight track and each cluster, weighted by the brightness of each cluster, was about 290 μm [19,21].

III. EVENT SELECTION OF STOPPED- Ξ^- REACTIONS

A total of 8000 (K^-, K^+) events above $p_{K^+} \geq 0.95 \text{ GeV}/c$ were scanned many times by eye and categorized according to their event topologies, defined by the number of charged prongs, kinks, and Λ particles. The rationale behind the high p_{K^+} selection is that the quasifree Ξ^- production is peaked at $\sim 1.1 \text{ GeV}/c$. Stopped- Ξ^- candidates were then selected by requiring that at the stopping point of a Ξ^- there exist either no further tracks (zero prong), or one, two, or three (stopping or interacting) charged prongs, as shown in Fig. 3. For instance, the survived Ξ^- -decay events belong to the one-prong configuration. We retained 874 events after scanning.

Due to the high momentum transfer ($\sim 0.55 \text{ GeV}/c$) in the elementary $K^- p \rightarrow K^+ \Xi^-$ process, most Ξ^- 's from the (K^-, K^+) reaction on free protons decay or range out before stopping in the SCIFI detector. However, it is possible to stop low-momentum Ξ^- 's produced from carbon in the SCIFI detector. We therefore imposed tight constraints on the selection of Ξ^- production from carbon nuclei: a coplanarity angle between Ξ^- and the (K^-, K^+) reaction plane is required, $|k_{K^-} \times k_{K^+} \cdot k_{\Xi^-}| > 0.1$, and the missing mass should be more than 15 MeV/c^2 off the known Ξ^- mass

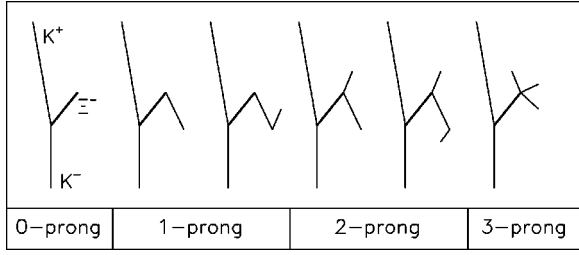


FIG. 3. Event configurations in terms of the number of charged prongs from the end point of the stopping Ξ^- .

($|m_X - m_{\Xi^-}| > 15 \text{ MeV}/c^2$), as shown in Fig. 4. A total of 334 events survived after imposing the coplanarity and missing mass cuts.

We then calculated the excitation energy E_{11B} relative to the mass of a $^{11}\text{B}(\text{g.s.})$ nucleus assuming a $^{12}\text{C}(K^-, K^+ \Xi^-)^{11}\text{B}^*$ reaction. The kinetic energy of the Ξ^- was measured using an empirical energy-range formula, approximated by $T_{\Xi^-}(\text{MeV}) = 38.183 \cdot R_{\Xi^-}^{4/7}(\text{cm})$. The excitation energy spectrum in Fig. 5 shows a significant peak at $E_{11B} = 0 \text{ MeV}$, and a broad bump above $E_{11B} = 50 \text{ MeV}$. The peak can be understood as a sum of the ground state ($3/2^-$), the $1/2^-$ state at 2.21 MeV, and the $3/2^-$ state at 5.02 MeV. The broad bump structure above 50 MeV is mainly due to background from in-flight Ξ^- decay and many other processes, which are discussed later. A small bump at $\sim 20 \text{ MeV}$ could be attributed to the 1 *s*-hole states observed in $^{12}\text{C}(p, 2p)^{11}\text{B}^*$ reaction [22].

Excitation spectra for different number of prongs at the Ξ^- stopping point are shown in the insets of Fig. 5. The broad bump structure could be kinematically attributed to two-step $(K^-, K^+ \Sigma)X$ processes ($\leq 1 \mu\text{b}/\text{sr}$ above $p_{K^+} = 0.95 \text{ GeV}/c$ [23]), nuclear evaporation, hypernuclear production reaction $(K^-, K^+ p)X$, in-flight free Ξ^- decays, and so on. We imposed $p_{K^+} > 1.1 \text{ GeV}/c$ to effectively suppress

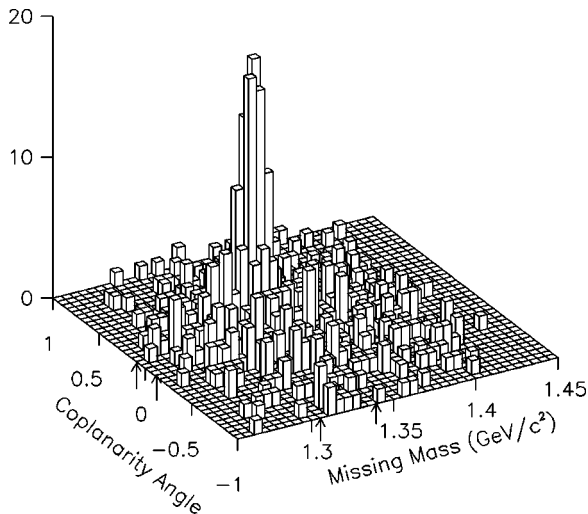


FIG. 4. Coplanarity angle and missing mass distribution assuming $p(K^-, K^+) \Xi^-$ reaction. A sharp peak represents the elementary $K^- p \rightarrow \Xi^- K^+$ scattering events. Arrows indicate the region that we selected events to optimize Ξ^- stopping efficiency.

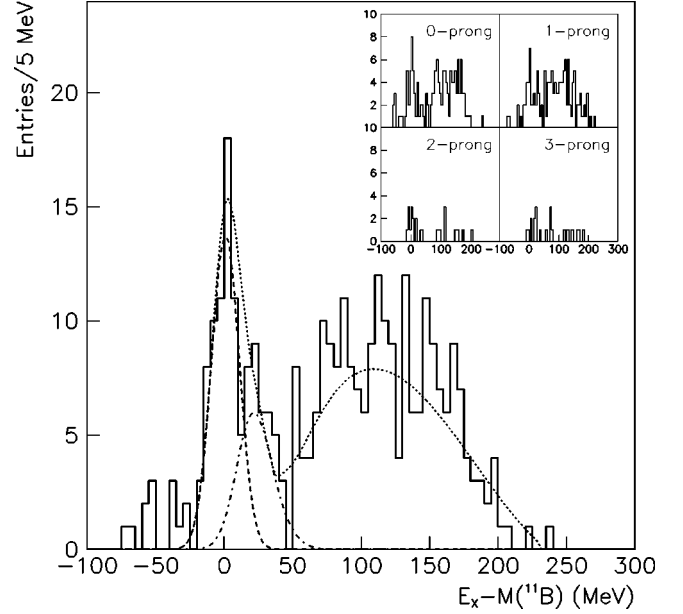


FIG. 5. Excitation energy spectrum for $K^-^{12}\text{C} \rightarrow K^+ \Xi^-^{11}\text{B}$ reaction relative to the mass of ^{11}B . Insets represent the excitation energy spectra with respect to the number of charged particles at the Ξ^- stopping point.

the background due to the broad bump structure. This cut was based on a Monte Carlo simulation. Events at around -50 MeV are possibly due to hypernuclear production with pion or proton emission, which were excluded by later constraints.

The abundance of the events, particularly for the zero-prong configuration, close to $0.95 \text{ GeV}/c$ supports a sizable contribution of two-step processes which are not associated with Ξ^- production. This background was considerably suppressed by requiring that $-20 < E_{11B} < 50 \text{ MeV}$, as shown in Fig. 6.

Due to nuclear evaporation, low-energy protons are possibly emitted from the (K^-, K^+) reaction vertex. Such low-energy protons leave a track of a few mm, so we imposed a minimum track length of 3 mm, which corresponds to about $T_p = 16 \text{ MeV}$. This cut was based on observation of low-energy protons in an emulsion plate [24]. Direct hypernuclear production from (K^-, K^+) reaction could result in emission of a proton or a pion in a hypernuclear decay. The proton or pion could be misidentified as a Ξ^- if it leaves a similar track length to that of the Ξ^- . In the absence of correlations, any direction with respect to the recoil momentum is equally likely. Therefore, we required that a stopping Ξ^- be observed in the forward direction ($\cos \theta_{\Xi^-} > 0$). We also exclude events in which a Ξ^- track is apparently less bright than a π^- track by requiring that the unit brightness ratio, $(dB/dx)_{\pi^-} / (dB/dx)_{\Xi^-} < 1.5$; the unit brightness is defined as the track density weighted by pulse height on each pixel. This is done in order to minimize the misidentification of π^- as Ξ^- for a very short Ξ^- decay followed by π^- interaction. Additionally, we required that $|m_{\Lambda \pi^-} - m_{\Xi^-}| > 15 \text{ MeV}/c^2$ for the one-prong events with a Λ and the three-prong events, in order to reject free Ξ^- decay events.

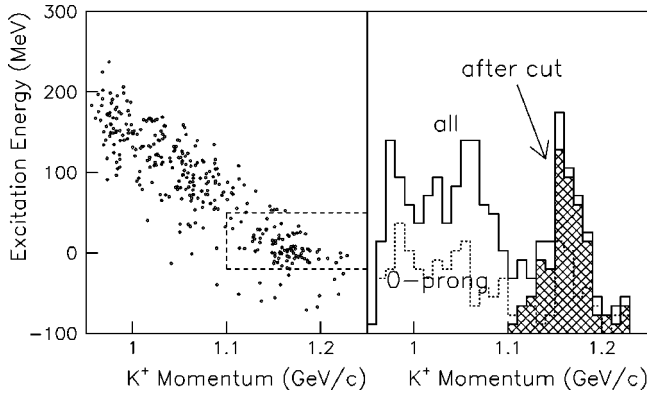


FIG. 6. Excitation energy versus K^+ momentum distribution (left) and the K^+ momentum distributions (right) are represented. Selected were the events in a dashed-line box. The K^+ momentum spectra of all event set and the zero-prong events are displayed as open histograms, while the spectrum after selection is shown as an overlaid hatched histogram.

After imposing all the requirements described above, 72 events were retained. We discuss below several background processes which could still reside in this final sample of stopping Ξ^- events (see Table I).

(1) In-flight $\Xi^-p/\Xi^-^{12}\text{C}$ inelastic scattering events could be misidentified as stopping Ξ^- events when occurred near the Ξ^- stopping vertices. The total yield for in-flight Ξ^- inelastic scattering processes can be written as $Y = N_{\Xi^-} \cdot N_A / W \cdot \rho \cdot \sigma_{abs} \cdot L$, where the effective target length L is set to 0.08 ± 0.04 cm, which is a typical error on track length measurement. We compared the measured track length with the generated length in the Monte Carlo simulation. The inelastic scattering cross section was adopted from Nijmegen-D model prediction, for example, $\sigma_{abs} = 177$ mb averaged over the region $0 \leq T_{\Xi^-} \leq 9$ MeV, where a Ξ^- has a maximum range of 0.08 cm. $N_A / W \cdot \rho$ indicates the number of target nucleons per cm^2 , which is $0.491 \times 10^{23} / \text{cm}^2$. N_A denotes Avogadro's number, W the atomic weight, and ρ the target density (1.06 g/cm^3). Out of the 72 stopping Ξ^- events, the background due to in-flight Ξ^- interaction was estimated to yield $0.21_{-0.09}^{+0.07}$ events, assuming that the effective proton number in a carbon nucleus is 3. The reported value of 20 ± 7 mb for the inelastic cross section [24] was based on observation of in-flight Ξ^- interactions with emulsion nuclei. The interacting Ξ^- particles were sampled before stopping, so that the measured cross section yields much

TABLE I. Background in the stopping Ξ^- event sample.

Background process	Number of events
$\Xi^-p/\Xi^-^{12}\text{C}$ in-flight interaction	$0.21_{-0.09}^{+0.07}$
$\pi^-p/\pi^-^{12}\text{C}$ interaction	3.7 ± 0.95
Free $\Xi^- \rightarrow \Lambda \pi^-$ decay	0.53 ± 0.53
Nuclear evaporation	0.89 ± 0.15
Hypernuclear production	$1.38_{-0.94}^{+0.22}$
K/π misidentification	none
Total background	$6.7_{-1.4}^{+1.1}$

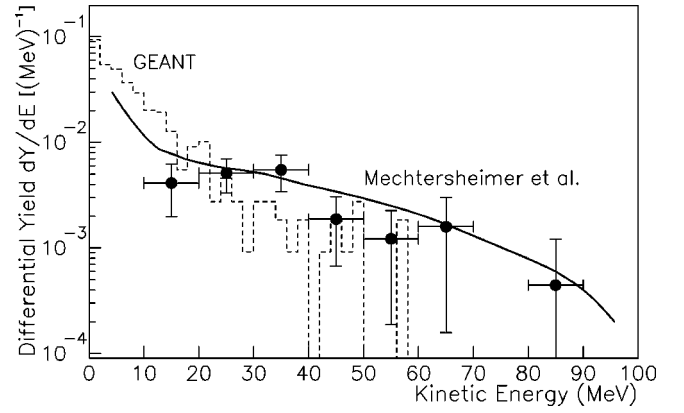


FIG. 7. The differential yield for charged particle emission per stopped- π^- is represented as closed circles overlaid by error bars. A solid line indicates an old measurement of the proton yield. Error bars in the old measurement are not shown here due to being negligibly small. Dotted line shows GEANT based simulation results. The total yield in the simulation is a factor of 2 smaller than our measurement in the region above 20 MeV.

smaller background than based on theoretical estimate. We therefore take $0.21_{-0.09}^{+0.07}$ events as being due to in-flight Ξ^- interactions.

(2) A low-energy π^- interaction could be mistaken as a stopping Ξ^- event. It would involve both an invisibly short Ξ^- decay and a π^- interaction immediately after the Ξ^- decay. We have nearly the same number of π^- particles as Ξ^- particles due to the 100% branching ratio of $\Xi^- \rightarrow \Lambda \pi^-$. The in-flight π^- interaction and the π^- absorption in a carbon nucleus were taken into account using a GEANT based simulation [25]. To our knowledge, there is one old measurement of the kinetic energy distribution of charged particles emitted following the absorption of stopped π^- in ^{12}C [26]. The proton multiplicity was reported to be 0.45 ± 0.04 , and the average kinetic energy 10.4 ± 1.8 MeV. These results are, however, different from the simulation results, particularly for the kinetic energy distribution. We therefore measured the differential yield of protons as a function of their kinetic energy. Out of 874 events, we first selected 226 events which are of one-prong track configuration, as shown in Fig. 3. We then required that the π^- should stop in a backward direction against the Ξ^- track. We finally retained 32 events as stopped- $\pi^-^{12}\text{C} \rightarrow pX$ events observed in the SCIFI target. We assumed all emitted particles to be protons. Using an empirical energy-range formula, approximated by $T_p(\text{MeV}) = 32.972 \cdot R_p^{4/7}(\text{cm})$, we plot the differential yield of the protons as a function of their kinetic energy in MeV, as shown in Fig. 7. Our results suggest that GEANT results should be scaled up by a factor of 2, to compensate for the discrepancy between the measurement and the simulation. Nevertheless, the background due to π^- interaction is found to be quite small. For example, the zero-prong configuration at a stopping Ξ^- track needs $\pi^-^{12}\text{C} \rightarrow$ neutrals following a very short π^- track. For the one-prong configuration, there should be a single charged-particle emission via π^- interaction. While the two-prong configuration needs two particle emission from either $\pi^-p/\pi^-^{12}\text{C}$ elastic scatterings or the

stopped- π^- absorption in ^{12}C , the multiprong configuration requires the multiprong emission after π^- interaction following a visibly short track of either Ξ^- or π^- . The total possible background yield is estimated to be 4.1% of the stopping Ξ^- events (3.2% of the one-prong and 0.21% of the two-prong configurations due to in-flight π^- interactions, plus 0.64% of the one-prong configuration associated with stopped- π^- absorption in ^{12}C) from a Monte Carlo simulation. If the background yield is corrected by the above factor, there would be 3.7 ± 0.95 events due to π^- interaction.

(3) When the Λ decays near the Ξ^- decay vertex, free Ξ^- decay could be misidentified as multiparticle emission from the stopped- Ξ^- reaction. Because we excluded one event for free Ξ^- decay followed by $\Lambda \rightarrow p\pi^-$ from the stopping Ξ^- event selection, there should be a background contribution of 0.53 ± 0.53 $\Lambda \rightarrow n\pi^0$ decay events.

(4) Background due to nuclear evaporation could remain in the stopping Ξ^- sample. The kinetic energy distribution of protons emitted via nuclear evaporation was reported by a recent KEK emulsion experiment [24]. With a 16-MeV cut, 2.48% of evaporation protons survived ($dN/dT_p = \text{const} \cdot e^{-0.2324 \cdot T_p}$, where T_p is given in MeV). We assume that all of the evaporation processes are due to the excited $^{11}\text{B}^*$ decays, therefore we take one-half of the events (36 events) in the stopping Ξ^- sample. The background due to nuclear evaporation was thus found to be 0.89 ± 0.15 events.

(5) Hypernuclear production from the (K^-, K^+) reaction could still exist in the stopping Ξ^- sample. A stopping proton or pion from the decay of a hypernucleus could be emitted in the backward direction, which results in a relatively large negative value of the excitation energy $E_{11\text{B}}$. Since we have no *a priori* knowledge of the proton or pion momentum distribution for hypernuclear decay, this background estimate relies on real data categorized as backward Ξ^- events. Reversing the sign of the polar angle with respect to the K^- beam track ($\cos \theta_{\Xi^-} \rightarrow -\cos \theta_{\Xi^-}$, where $\cos \theta_{\Xi^-}$ is negative) for each event, we made a random rotation with respect to the beam direction. The background yield was then estimated to be $1.38_{-0.94}^{+0.22}$ events by requiring $-20 < E_{11\text{B}} < 50$ MeV. The errors quoted indicate uncertainty in sampling real data for hypernuclear production.

(6) K/π misidentification may be involved in the background, but we have observed no event due to Σ^- production in the missing mass spectrum. These would result from (π^-, K^+) and (K^-, π^+) reactions in the stopping Ξ^- sample. To obtain some confidence regarding the event selection, we calculated the fraction of the stopping Ξ^- in the $(K^-, K^+ \Xi^-)$ reaction with the SCIFI target. We adopted the harmonic oscillator nuclear model, the measured K^- beam momentum, and (K^-, K^+) vertex distributions. The observed Ξ^- momentum distribution was reproduced by the Monte Carlo simulation. The stopping fraction of the Ξ^- was found to be 1.34% in the simulation, whereas in the data $1.19 \pm 0.15\%$ of 5.5×10^3 tagged Ξ^- particles, or 65.3 events survived. In the Monte Carlo simulation we used an escaping probability of the Ξ^- from ^{12}C from our previous analysis,

TABLE II. Number of charged particles from the end point of a stopping Ξ^- track.

	zero-prong	one-prong	two-prong	three-prong
E176 (emulsion)	53%	27%	14%	6%
This experiment	46%	28%	14%	12%

0.801 ± 0.024 . Our event selection therefore shows a good statistical consistency between simulation and measurement. We also compared the observed ratio of the event configuration with recent KEK-E176 experimental results [27]. We made an efficiency correction due to the different spatial resolution between the emulsion plate and the SCIFI detector. As shown in Table II, both experimental results are very consistent, but the emulsion has of course a different target composition.

IV. HYPERNUCLEUS FORMATION IN STOPPED- $\Xi^-^{12}\text{C}$ REACTIONS

Stopped- $\Xi^-^{12}\text{C}$ reactions are possibly characterized by either low-energy Λ emission or nearly monoenergetic π^- emission in sequential weak decays of hypernuclei. All possible decay channels of the highly excited double- Λ hypernuclear state, $^{13}_{\Lambda\Lambda}\text{B}^*$ ($\Xi^- + ^{12}\text{C}$ atomic system), with the excitation energy up to 40 MeV are represented in Ref. [16] with respect to hypernuclear species. Observation of Λ particle emission should then give quantitative information on the formation probability of double and single hypernuclei (see Table III).

Out of the stopping Ξ^- event sample, we observed 16 Λ decays with the V -decay configuration. When both proton and pion tracks are identifiable (track length > 1 mm), the Λ decay configuration is defined as a V decay. Another four Λ decays were selected from the two- and three-prong configuration. These are responsible for very short Λ decays from stopped- Ξ^- reaction vertices. We calculated an invariant mass of $p\pi^-$ in a combinatorial way and the four events satisfied the Λ decay configuration ($|m_{p\pi^-} - m_{\Lambda}| < 15$ MeV/ c^2). We also analyzed nine straight tracks without other particle tracks, hypothesizing that these are low-energy Λ decays with invisibly short proton tracks. The Λ momenta were determined using kinematic constraints of the measured π^- decay angles and momenta, compared with Monte Carlo simulation results. Out of nine tracks, eight tracks were found to be consistent with π^- tracks due to low-energy Λ decays. We therefore observed a total of 28 Λ decays. We retained 26 events and two events having two Λ decays among them.

The detection efficiency was calculated by a Monte Carlo simulation, as shown in Fig. 8. We generated Λ randomly

TABLE III. Formation probabilities of hypernuclei in stopped- $\Xi^-^{12}\text{C}$ reactions.

Channel	double- Λ /twin- Λ	single- Λ	$\Lambda\Lambda + X$
Ratio	$18 \pm 13\%$	$65 \pm 6\%$	$17 \pm 12\%$

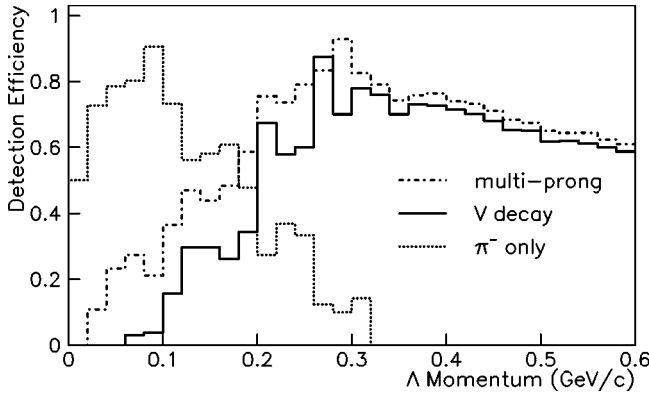


FIG. 8. Detection efficiencies for Λ decays with respect to the track configuration are represented as different lines.

emitted from the end point of a stopping Ξ^- , so that we made exactly the same event configuration as for real data. The simulated event set was classified into two groups of events with respect to the Λ decay track configuration by scanning. The detection efficiency was found to drop to nearly zero below 0.1 GeV/c by requiring that the Λ decay be accompanied by visible proton and pion decay tracks, while the efficiency was still high enough to detect the Λ decay with only a decay π^- track, even in the same momentum region. Out of 16 Λ decays with the V-track configuration, there were four events below 0.1 GeV/c. For these events the decay proton tracks were not positively determined due to the short track length and the small decay angle. Instead of introducing additional constraints, we altered the Λ decay configuration for those four events into the straight π^- track configuration, in order to avoid systematic uncertainties in the region where the detection efficiency is very low.

Figure 9 shows a Λ momentum distribution for the stopped- $\Xi^-^{12}\text{C} \rightarrow \Lambda X$ reaction. Overlaid lines represent theoretical estimates of the AMD (plus QL method) model for differential yield of Λ emission per stopped- $\Xi^-^{12}\text{C}$ reaction [17]. The arrows indicate characteristic Λ momenta of the particular channels shown in the figure. Kinematically, the $\Xi^-^{12}\text{C} \rightarrow \Lambda + {}_{\Lambda}^{12}\text{B}(1^-)$ reaction produces the most energetic Λ hyperon of 0.223 GeV/c, although the $\Xi^-^{12}\text{C} \rightarrow \Lambda + {}_{\Lambda}^{12}\text{B}^*(2^+)$ reaction is predicted to be dominant, accompanied by a Λ of about 0.164 GeV/c. However, we did not impose any constraint on the maximum Λ momentum, because the Λn and $\Sigma^0 n$ weak decays of a bound H -dibaryon could yield a high momentum Λ particle above the end point (0.223 GeV/c) for hypernuclear formation. Nonmesonic $\Lambda\Lambda \rightarrow \Lambda N$ decays are possible as well.

Free Ξ^- decays at rest in the stopping Ξ^- sample should be taken into account. Some fraction of the Ξ^- captured in an atomic orbit of ${}^{12}\text{C}$ could decay during an atomic cascade. Such a free stopped- Ξ^- decay should show collinear Λ and π^- tracks in the lab system, and both decay products should be monoenergetic at 0.139 GeV/c. However, we found no such events for the stopped- Ξ^- decay. The time taken for the Ξ^- atomic cascade is predicted to be relatively short ($\sim 10^{-12}$ s) in atoms with $Z > 2$, and only a few ($< 1\%$) of

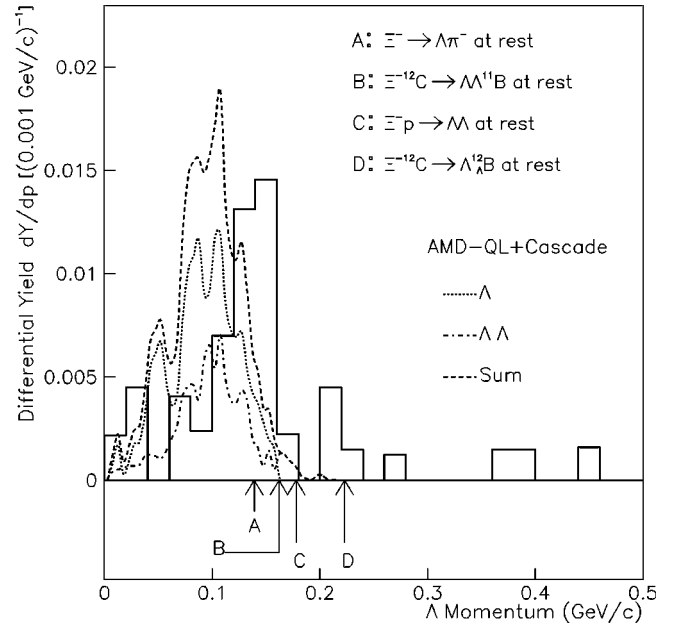


FIG. 9. Λ momentum distribution for $\Xi^-^{12}\text{C} \rightarrow \Lambda X$ reaction. Overlaid lines represent theoretical estimates of differential yield for one and two Λ emission probabilities and their sum.

the Ξ^- are expected to decay during the process [28,29]. Our result is thus consistent with this theoretical estimate.

The yields for the Ξ^- capture reactions can be written as $Y_i = \Gamma_i / (\Gamma_0 + \Gamma_1 + \Gamma_2)$, where Γ_i are the partial rates for the final channels, $\Lambda + \Lambda + X$ (Γ_2), ${}_{\Lambda}^A Z + \Lambda + X$ (Γ_1), ${}_{\Lambda\Lambda}^{A'} Z' + X$ (Γ_0). With two observed $\Lambda\Lambda$ events Y_2 is estimated to be $17 \pm 12\%$. The Λ momenta for the $\Xi^-^{12}\text{C} \rightarrow \Lambda\Lambda X$ reaction were all observed to be below the end point, for the $\Xi^-^{12}\text{C} \rightarrow \Lambda\Lambda^{11}\text{B}$ reaction, 0.162 GeV/c. The yield for single Λ decay, Y_1 , was then found to be $65 \pm 6\%$ integrated over the region below 0.223 GeV/c. This yield is attributed to the single- Λ hypernuclear formation through $(\Xi^-, {}^{12}\text{C})$ atomic states. The formation probability for double- Λ /twin- Λ hypernuclei is given by $1 - Y_1 - Y_2$, and found to be $18 \pm 13\%$. Some data points above 0.223 GeV/c yield 14%, which are possibly kinematically attributed to the $H \rightarrow \Lambda n$ decay and the nonmesonic $\Lambda\Lambda \rightarrow \Lambda N$ decays of double- Λ hypernuclei. There are, however, $6.7_{-1.4}^{+1.1}$ background events in the stopping Ξ^- event sample, as discussed in the previous section. Although the background contribution was taken into account when calculating the number of stopping Ξ^- particles, its fraction still remains as 4.8% of the total data.

A peak structure is observed at 0.132 GeV/c (from a Gaussian fit) in Fig. 9. Although the mean of this peak is closer to 0.139 GeV/c (reaction A), reaction A is ruled out since the recoil pion is too energetic to stop in the SCIFI detector and events of this sort are rejected. The peak position is about 0.05 GeV/c higher than that predicted by the AMD-QL model calculation [17]. One of two Λ particles for the $\Xi^-^{12}\text{C} \rightarrow \Lambda\Lambda X$ reaction lies on the peak for both of the observed events. The formation probability integrated over the region $0.2 < p_{\Lambda} < 0.223$ GeV/c yields $9.4 \pm 5.3\%$, to which only $\Xi^-^{12}\text{C} \rightarrow \Lambda + {}_{\Lambda}^{12}\text{B}(1^-)$ could be attributed kinematically. However, the measured formation probability is

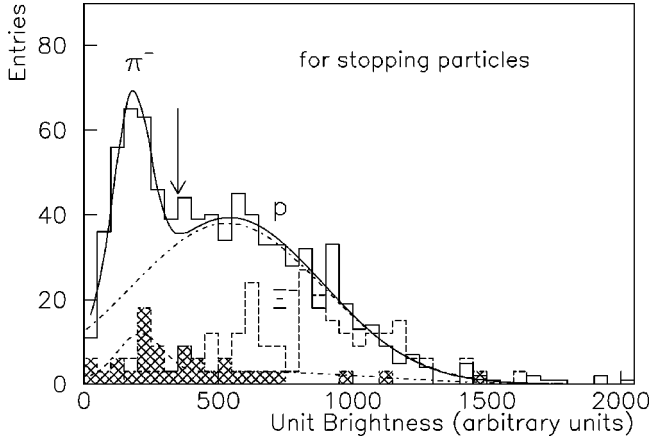


FIG. 10. The unit brightness (dB/dx) distributions for stopping particle (π^- , p , and Ξ^-) tracks. The dB/dx of stopping Ξ^- tracks is shown as a dashed histogram with an overlaid fitted line. Hatched area indicates a sample of stopping particles emitted from the stopping point of Ξ^- .

considerably larger than the level predicted by theoretical calculations. A theoretical estimate of the doorway double- Λ hypernuclear picture gives 0.25% for the $\Xi^-^{12}\text{C} \rightarrow \Lambda + {}^{12}\text{B}(1^-)$ and 0.67% for ${}^{12}\text{B}(2^+)$, in case of a Ξ^- -nucleus potential of $V_{0\Xi^-} = 16$ MeV and $(3d)_{\Xi^-}$ atomic capture [16]. Another estimate of the AMD-QL model calculation [17] for $\Xi^-^{12}\text{C} \rightarrow \Lambda + {}^{12}\text{B}$ channel gives 3.24%, while for the $\Xi^-^{12}\text{C} \rightarrow \Lambda + n + {}^{11}\text{B}$ channel, it is 20.9%.

In order to identify hypernuclear species, we measured the momentum of a charged particle emitted from the stopping point of the Ξ^- . Since protons may come out of the hypernuclear decays, good π/p separation is necessary. The track brightness per unit length is proportional to the kinetic energy that a particle lost along the track length. We measured the unit brightness (dB/dx) averaged over the track length which corresponds to 4 mm in Z direction (except for the first 1 mm from the stopping point) for XZ and YZ images, respectively. We then added them up with a correction factor ($YZ/XZ = 0.793$) corresponding to the difference of the IIT gain between XZ and YZ images. Figure 10 represents the unit brightness distributions of stopping particle tracks: π^- and p tracks sampled from Λ decays, and Ξ^- tracks from the stopping Ξ^- events. Reasonable π/p separation is possible by requiring that the unit brightness be less than 350 (in arbitrary units), as indicated by an arrow in Fig. 10.

The kinetic energy spectrum of π^- from the stopping Ξ^- is shown in Fig. 11. While the cross data points represent the kinetic energies of particles before π/p separation, the histogram shows those of the pions retained after π/p separation. Uncertainty in π/p separation is due to low-brightness proton tracks misidentified as pion tracks, which yield about 18% of the selected π^- tracks.

The detection efficiency was evaluated using a Monte Carlo simulation. It is nearly zero above $T_{\pi^-} = 40$ MeV, solely due to the finite size of the SCIFI detector. There still remains some yield in the region between 24 and 40 MeV, in which many of the characteristic pionic decays of double- Λ

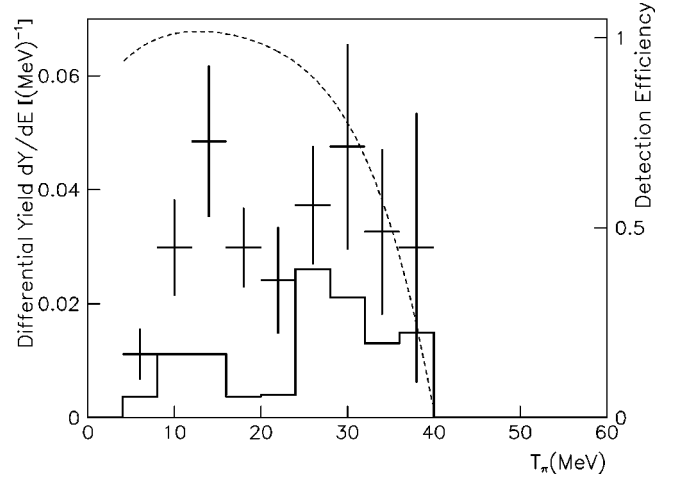


FIG. 11. Kinetic energy spectrum of π^- from the stopping Ξ^- . While the cross data points represent the kinetic energies of particles before π/p separation, the histogram shows those of the pions retained after π/p separation. A dashed line indicates the π^- detection efficiency.

hypernuclei are anticipated, as quoted in Table IV. Three events with two pion decays remained; two of them contain low-energy pions, while the third has pions of 27.8 ± 0.9 MeV and 29.9 ± 0.9 MeV, respectively. The latter event could be a candidate for the sequential weak decay of ${}^6_{\Lambda\Lambda}\text{He} \rightarrow {}^5_{\Lambda}\text{He} + p + \pi^-$ ($T_{\pi^-} = 29.5$ MeV, if $\Delta B_{\Lambda\Lambda} = 4.7$ MeV [30]) followed by the ${}^5_{\Lambda}\text{He} \rightarrow {}^4\text{He} + p + \pi^-$ decay ($T_{\pi^-} = 31.7$ MeV taken from experimental data [31]). It could also be a candidate for the sequential decay of ${}^5_{\Lambda\Lambda}\text{He} \rightarrow {}^4_{\Lambda}\text{He} + p + \pi^-$ ($T_{\pi^-} = 30.3$ MeV, if $\Delta B_{\Lambda\Lambda} = 0.22$ MeV [30]) followed by the ${}^4_{\Lambda}\text{He} \rightarrow {}^3\text{He} + p + \pi^-$ decay ($T_{\pi^-} = 30.5$ MeV taken from experimental data [32]). The characteristic π^- kinetic energy indicates the most probable energy in the three-body decay spectrum. In the above decay sequence the decay proton could have too low a kinetic energy (several MeV) for us to detect.

The event with two pion emission is shown in Fig. 12. It should be noted that the observed event is almost background free from free Ξ^- and Λ decays. Nevertheless, it cannot give conclusive evidence for the ${}^6_{\Lambda\Lambda}\text{He}$ or ${}^5_{\Lambda\Lambda}\text{He}$ decay due to uncertainty in π^-/p separation and its three body decay sequence.

We also looked for the nonmesonic decay of double hypernuclei involving Σ^- , for instance, the ${}^6_{\Lambda\Lambda}\text{He} \rightarrow {}^4\text{He} + p + \Sigma^-$ decay [33,34]. The $\Lambda\Lambda \rightarrow \Sigma^- p$ decay can be characterized as one stopping track and one kink track. However, we observed no events with both Σ^- and proton. If the proton and the residual nucleus form a single particle like ${}^5_{\Lambda\Lambda}\text{He} \rightarrow {}^4\text{He} + \Sigma^-$, only the Σ^- decay can be observed. Events with a two-kink track (the second configuration of the one-prong event in Fig. 3) were then sampled as candidates for the nonmesonic Σ^- decays of double- Λ hypernuclei. Assuming $\Sigma^- \rightarrow n\pi^-$ decay, the Σ^- momentum was reconstructed. Two events ($T_{\Sigma^-} = 44, 55$ MeV) were retained after imposing that the unit brightness of the Σ^- track should be greater than that of the π^- track. Although these two events

TABLE IV. Characteristic π^- kinetic energies for hypernuclear decays [4,15,29–31]. The $\Lambda\Lambda$ bond energies ($\Delta B_{\Lambda\Lambda}$) are input in the case of double Λ hypernuclear decays. Uncertainties in $\Delta B_{\Lambda\Lambda}$ give only a several-MeV change in the π^- kinetic energy spectrum. For three-body decays, the quoted values indicate the most probable energy.

Decay	T_π (MeV)	$\Delta B_{\Lambda\Lambda}$ (MeV)	Decay	T_π (MeV)
${}^4_{\Lambda\Lambda}H \rightarrow {}^4_\Lambda\text{He} + \pi^-$	43.4	0.24	${}^3_\Lambda H \rightarrow {}^3\text{He} + \pi^-$	40.7
${}^5_{\Lambda\Lambda}H \rightarrow {}^5_\Lambda H + \pi^-$	53.9	0.92	${}^4_\Lambda H \rightarrow {}^4\text{He} + \pi^-$	53.2
${}^5_{\Lambda\Lambda}\text{He} \rightarrow {}^4_\Lambda\text{He} + p + \pi^-$	30.3	0.22	${}^4_\Lambda\text{He} \rightarrow {}^3\text{He} + p + \pi^-$	30.5
${}^6_{\Lambda\Lambda}\text{He} \rightarrow {}^5_\Lambda\text{He} + p + \pi^-$	29.5	4.7	${}^5_\Lambda\text{He} \rightarrow {}^4\text{He} + p + \pi^-$	31.7
${}^7_{\Lambda\Lambda}\text{He} \rightarrow {}^7_\Lambda\text{Li} + \pi^-$	34.6	4.1	${}^7_\Lambda\text{He} \rightarrow {}^7\text{Li} + \pi^-$	41.4
${}^8_{\Lambda\Lambda}\text{Li} \rightarrow {}^8_\Lambda\text{Be} + \pi^-$	33.2	4.3	${}^7_\Lambda\text{Li} \rightarrow {}^7\text{Be} + \pi^-$	36.8
${}^{10}_{\Lambda\Lambda}\text{Be} \rightarrow {}^{10}_\Lambda\text{B} + \pi^-$	25.5	4.3	${}^{11}_\Lambda\text{B} \rightarrow {}^{11}\text{C} + \pi^-$	35.1
${}^{11}_{\Lambda\Lambda}\text{Be} \rightarrow {}^{11}_\Lambda\text{B} + \pi^-$	32.5	4.6	${}^{12}_\Lambda\text{C} \rightarrow {}^{12}\text{N} + \pi^-$	26.6
${}^{12}_{\Lambda\Lambda}\text{B} \rightarrow {}^{12}_\Lambda\text{C} + \pi^-$	31.0	4.7	$\Xi^- \rightarrow \Lambda + \pi^-$	57.4
${}^{13}_{\Lambda\Lambda}\text{B} \rightarrow {}^{13}_\Lambda\text{C} + \pi^-$	36.3	4.8	$\Lambda \rightarrow p + \pi^-$	32.5

were not reproduced by the hypothesis of the Ξ^- - ${}^{12}\text{C}$ interaction followed by the $\Xi^- \rightarrow \Lambda \pi^-$ decay (0.21 events as quoted in the Sec. III), the unit brightness of the Σ^- tracks were also less than the value we imposed for π/p separation. We therefore do not take them as candidates for the nonmesonic Σ^- decays of double- Λ hypernuclei, but as being due to possible π^- interactions. Unless the detection system is able to detect hypernuclear fragments, detecting neutrons is essential to experimentally confirm the $\Lambda\Lambda \rightarrow \Sigma^- p$ nonmesonic decays of double hypernuclei.

V. H-DIBARYON FORMATION FROM Ξ^- CAPTURE ON ${}^{12}\text{C}$

The decays of the H dibaryon via the Ξ^- capture reaction $\Xi^- {}^{12}\text{C} \rightarrow HX$ were thoroughly looked for in the SCIFI target. Unlike the H search through direct production, the experimental sensitivity and acceptance depend crucially on the lifetime and the decay modes of the H since the H is detected via its decay products. A bound H decays into ΛN , ΣN , and $\Lambda N \pi$ channels via $\Delta S=1$ weak decays in the mass region between the ΛN and the $\Lambda\Lambda$ thresholds. Theoretical calculations of Donoghue *et al.* [35] predict S -wave $\Delta S=1$ H life-

times of several $\times 10^{-9}$ s for an H mass near the $\Lambda\Lambda$ mass to several $\times 10^{-7}$ s for an H mass near the Λn mass, and the factor of 2 decrease in H lifetimes is possible due to the P wave.

Since no H candidate was observed, we investigated our experimental sensitivity and acceptance in detecting the three decay modes, Λn , $\Sigma^- p$, and $\Lambda p \pi^-$, in order to set upper limits on the production rate of the H dibaryon assuming all of the H decays weakly via each one of the decay modes. The upper limits on the production rate of the H dibaryon through the reaction $\Xi^- {}^{12}\text{C} \rightarrow HX$ can then be written as $R = \Gamma_{\Xi^- {}^{12}\text{C} \rightarrow HX} / \Gamma_{\text{tot}} = (\mu_1, \mu_2) / \eta \cdot N_{\Xi^-}$, where (μ_1, μ_2) is 90% confidence level intervals for the Poisson signal mean μ [36,37], and η represents the detection efficiency. N_{Ξ^-} denotes the number of stopped- Ξ^- events.

A. $H \rightarrow \Lambda n$

Because the $H \rightarrow \Lambda n$ decay is characterized by a decay vertex shared with two neutral particles, one needs to tag a neutron to reconstruct this decay channel when the H lives long enough to separate its production and decay vertices within the detection resolution. Since we did not detect neutrons, we relied on only Λ decay kinematics for the $H \rightarrow \Lambda n$ search. For $m_H \sim 2m_\Lambda$, most of the 12.3 MeV energy released in $\Xi^- {}^{12}\text{C} \rightarrow H {}^{11}\text{B}$ reaction goes to the H . If the H decays within its flight length of ~ 1 mm, its Λ decay can be reconstructed from the end point of a stopping Ξ^- particle track. This analysis is essentially the same as described in the previous section for hypernuclear formation study.

In the Λ momentum spectrum of Fig. 9 there are several Λ particles observed beyond the region allowed for hypernuclear production. These events could be due to $H \rightarrow \Lambda n$ decay above 0.223 GeV/c, which would accept 92% of the simulated H events over the mass region below $\Lambda\Lambda$ threshold. However, as mentioned in the previous section, the $\Lambda\Lambda \rightarrow \Lambda N$ nonmesonic decay of double- Λ hypernuclei could also yield such a high-momentum Λ , beyond the momentum region for hypernuclear weak decay. We therefore did not take these events as candidates for the $H \rightarrow \Lambda n$ decay.

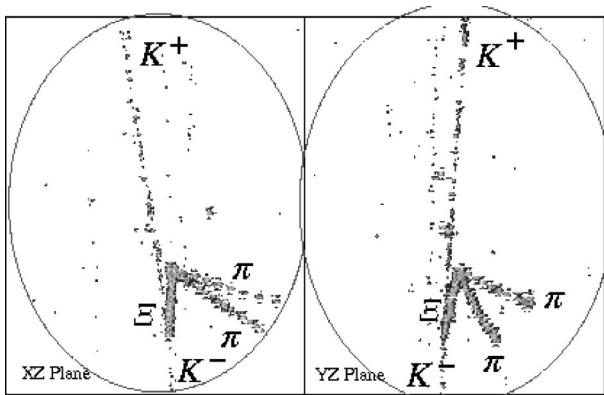


FIG. 12. A SCIFI image of a possible candidate for the characteristic pionic decays of the ${}^6_{\Lambda\Lambda}\text{He}$.

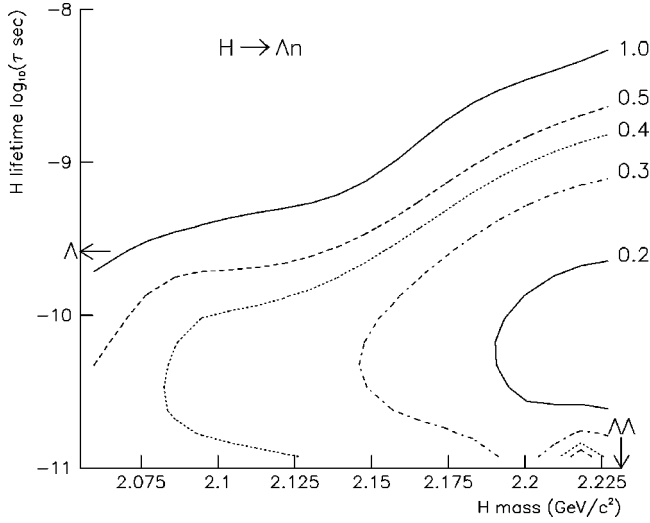


FIG. 13. Upper limits on the branching ratio of $\Xi^{-12}\text{C} \rightarrow HX$ assuming that all of the H decay into Λn .

For an H with longer lifetimes, the $H \rightarrow \Lambda n$ decay is seen as a momentum-unbalanced Λ decay with respect to a straight line connecting the $\Xi^{-12}\text{C}$ reaction vertex and the Λ decay vertex. No such event was observed in the stopping Ξ^- event sample. From this result, we set upper limits on the H production rate through the $\Xi^{-12}\text{C}$ reaction at rest. The detection acceptance was investigated in a detailed detector simulation. We required that one of the Λ decay products should stop in the SCIFI detector. The upper limits on the H production rate at 90% confidence level are shown in Fig. 13 as a function of the H mass ($m_{\Lambda n} \leq m_H \leq 2m_{\Lambda}$) and the H lifetime ($10^{-11} \leq \tau_H \leq 10^{-8}$ s). In the calculation, we assumed 100% branching ratio for the $H \rightarrow \Lambda n$ decay.

B. $H \rightarrow \Lambda p \pi^-$

The pionic weak decay of the H -dibaryon was searched for in the mass region between 2.194 GeV/c^2 ($\Lambda p \pi^-$) and 2.231 GeV/c^2 ($\Lambda \Lambda$). The event configuration of the $H \rightarrow \Lambda p \pi^-$ is very similar to the $\Lambda \Lambda$ production at the stopped- $\Xi^{-12}\text{C}$ reaction. However, we observed no events in which one V decay is due to a Λ decay and the other due to proton and pion from the $H \rightarrow \Lambda p \pi^-$ decay. For a very short-lived H , the decay $H \rightarrow \Lambda p \pi^-$ resembles the two-prong configuration with a Λ decay. One event was found to satisfy this constraint on the event configuration, but the reconstructed H masses (2.253, 2.268 GeV/c^2 for switching π^-/p assignment) were both above the $\Lambda \Lambda$ threshold.

Since no $H \rightarrow \Lambda p \pi^-$ decay was seen, we set upper limits on the production rate of the H dibaryon through the reaction $\Xi^{-12}\text{C} \rightarrow HX$ assuming that all of the H decay into $\Lambda p \pi^-$. We made a GEANT simulation [25] for this Monte Carlo study. We generated stopping Ξ^- particles with the measured vertex distribution, and produced the H and the residual nucleus $^{11}\text{B}(\text{g.s.})$. All H decay into $\Lambda p \pi^-$, equally in all phase space using a GENBOD routine [38]. The mass and lifetime ranges investigated were $m_{\Lambda p \pi^-} \leq m_H \leq m_{\Lambda \Lambda}$ and $10^{-11} \leq \tau_H \leq 10^{-8}$ s. We imposed that all charged track should be longer than 2 mm. Since the H in this decay mode

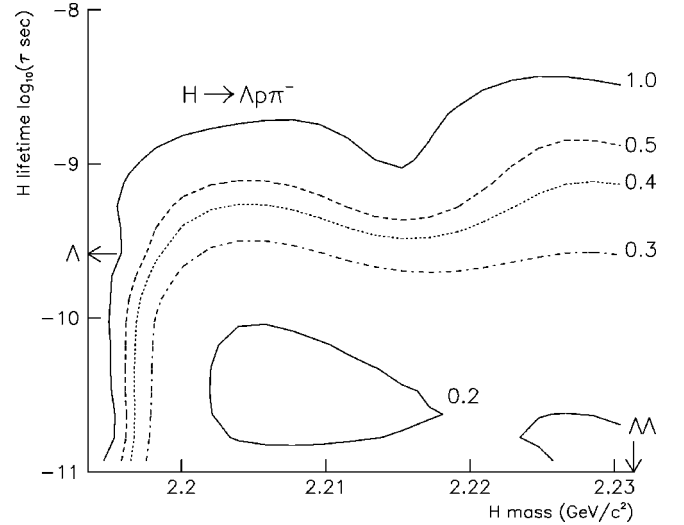


FIG. 14. Upper limits on branching ratio of $\Xi^{-12}\text{C} \rightarrow HX$ assuming that all of the H decay into $\Lambda p \pi^-$.

has very small phase space available, all decay products carry very low momenta and therefore leave very short tracks. The slope of the upper limits toward longer lifetimes in Fig. 14 is attributed to our finite SCIFI detector volume. Close to the $\Lambda p \pi^-$ threshold, detecting all three particles is far beyond our detector resolution, so that no upper limits are quoted. We took into account the decay branching ratio of $\Lambda \rightarrow p \pi^-$ (0.639). The result is shown in Fig. 14, and numbers represent the upper limits on the H production at 90% confidence level.

C. $H \rightarrow \Sigma^- p$

The $H \rightarrow \Sigma^- p$ decay is uniquely observed as a V track with a kink from the $\Sigma^- \rightarrow n \pi^-$ decay vertex. We reported in our previous analysis upper limits of 0.6–0.7% for the $H \rightarrow \Sigma^- p$ decay via direct production in $^{12}\text{C}(K^-, K^+ H)X$ [39]. For the stopped- $\Xi^{-12}\text{C}$ reaction, the decay vertex pointing back to the Ξ^- track was looked for. No such event was seen among the stopping Ξ^- sample. This result leads us again to set upper limits on the H production rate via stopped- Ξ^- reaction. We generated $H \rightarrow \Sigma^- p$ decays using a GEANT simulation. We then investigated the decay configuration in terms of the H mass ($m_{\Sigma^- p} \leq m_H \leq 2m_{\Lambda}$) and the H lifetime ($10^{-11} \leq \tau_H \leq 10^{-8}$ s). The decay proton should stop in the SCIFI target. It is not necessary to observe the H decay vertex separately from its production vertex. The upper limits on the H production rate at the 90% confidence level are shown in Fig. 15.

Our SCIFI detector is sensitive to a wide range of the H lifetimes from 10^{-11} s to a few 10^{-9} s. This range of lifetimes has been probed for the first time in our experiment, and our results are complementary with two recent long-lived H searches. One had a lifetime coverage from $\sim 5 \times 10^{-10}$ s to $\sim 1 \times 10^{-3}$ s [40] for $H \rightarrow \Lambda p \pi^-$, while the other had a coverage of several ns for the $H \rightarrow \Lambda n$ and $H \rightarrow \Sigma^0 n$ decays [41]. Since their results ruled out the H lifetimes predicted in Ref. [35], our detection sensitivity is unique to shorter H lifetimes of $10^{-11} \sim 10^{-9}$ s, which covers

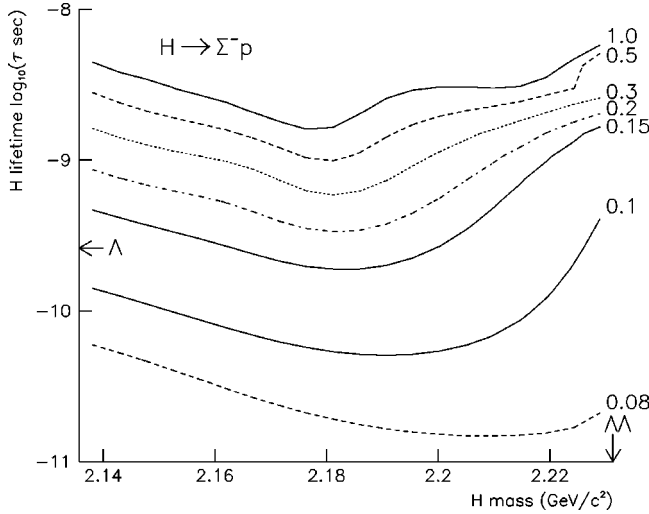


FIG. 15. Upper limits on the branching ratio of $\Xi^{-12}\text{C} \rightarrow HX$ assuming that all of the H decay into $\Sigma^- p$.

typical hyperon lifetimes. Our experimental sensitivity is almost constant over the H mass interval.

Although our results cannot be compared directly with the estimates of Aerts and Dover [10] due to different target nuclei, our upper limits close to $2m_\Lambda$ give a meaningful constraint on the existence of a bound H . The theoretical estimate shows that the H production ratio from the $\Xi^{-4}\text{He}$ atom approaches 1.0 near the $\Lambda\Lambda$ threshold (>0.5 above $m_H \sim 2.18 \text{ GeV}/c^2$ using a Nijmegen- D model for the P state of the $\Xi^{-4}\text{He}$ atom). Our results rule out such a large branching ratio for the H production from the $\Xi^{-12}\text{C}$ atom. The branching ratios of the order of 10^{-1} at $m_H \approx 2m_\Lambda$ give a more stringent constraint on the existence of the H , compared to theoretical estimates [10].

VI. CONCLUSIONS

Stopped- $\Xi^{-12}\text{C}$ reactions have been investigated with respect to H -dibaryon and hypernucleus formation with a

scintillating fiber detector. Out of 5.5×10^3 tagged Ξ^- particles via the (K^-, K^+) reaction, we obtained 72 stopping Ξ^- events with $6.7_{-1.4}^{+1.1}$ background events. We selected tagged stopping Ξ^- events by reconstructing the $^{12}\text{C}(K^-, K^+ \Xi^-)^{11}\text{B}$ reaction. Hypernuclear production was studied by observing free Λ decays in the stopped- Ξ^- reactions. From the observed Λ momentum spectrum, we found hypernuclear production rates of $18 \pm 13\%$, $65 \pm 6\%$, and $17 \pm 12\%$ for double/twin- Λ hypernucleus, single- Λ hypernucleus, and no hypernucleus cases, respectively. With the same sample of stopping Ξ^- events, we set upper limits on the H -dibaryon production rates through Ξ^- atomic capture in ^{12}C by searching for Λn , $\Lambda p \pi^-$, and $\Sigma^- p$ weak decays. The upper limits on $R(\text{stopped-}\Xi^{-12}\text{C} \rightarrow HX / \text{stopped-}\Xi^{-12}\text{C} \rightarrow \text{all})$ for an H decaying into Λn , $\Sigma^- p$, and $\Lambda p \pi^-$ were determined just below the $\Lambda\Lambda$ mass threshold in the H lifetime range $10^{-11} \leq \tau_H \leq 10^{-8}$ s. The upper limits on R for the Λn channel near the $2m_\Lambda$ threshold are set ~ 0.2 at 90% confidence level. For the $\Lambda p \pi^-$ channel, our detection resolution limits do not allow to probe the H mass region very close to the $\Lambda p \pi^-$ threshold. In other regions upper limits of ~ 0.2 – 0.3 are found for H lifetimes shorter than τ_Λ . The experimental sensitivity to $H \rightarrow \Sigma^- p$ decay is almost constant over the H mass region, and upper limits on R are found to be ~ 0.1 for $\tau_H \sim 10^{-10}$ s. Our results give tight constraints on the existence of a bound H , in comparison with the theoretical estimates of Aerts and Dover [10], albeit with different target nuclei.

ACKNOWLEDGMENTS

We would like to thank the staff of the KEK proton synchrotron for their continuous support. We also thank Prof. T. Motoba and Dr. A. Ohnishi for valuable discussions and for providing us with theoretical calculation results. This work was supported in part by a Grant-in-Aid for Scientific Research (08239103), the Ministry of Science, Culture and Education, Japan.

- [1] R.L. Jaffe, Phys. Rev. Lett. **38**, 195 (1977); **38**, 617(E) (1997).
- [2] C. Guaraldo, Proceedings of the Winter School II Course on Hadronic Physics at Intermediate Energy, Folgaria, 1987; LNF-87/21(P), 1987.
- [3] R.E. Chrien, Proceedings of International Conference on Quark Lepton Nuclear Physics, QULEN'97, Osaka, Japan, 1997; B. Bassalleck, Proceedings of the 6th Conference on the Intersections of Particle and Nuclear Physics, Big Sky, Montana, 1997.
- [4] S. Aoki *et al.*, Prog. Theor. Phys. **85**, 1287 (1991).
- [5] P. Beillière *et al.*, Phys. Lett. **39B**, 671 (1972); G. Wilquet *et al.*, *ibid.* **57B**, 97 (1975).
- [6] B. Povh, in *Properties and Interactions of Hyperons, Proceedings of the U.S.-Japan Seminar, Maui, Hawaii*, 1993, edited by B.F. Gibson, P.D. Barnes, and K. Nakai (World Scientific, Singapore, 1994).
- [7] G. Alexander *et al.*, Phys. Lett. B **384**, 377 (1996).
- [8] J.K. Ahn *et al.*, Phys. Lett. B **444**, 267 (1998).
- [9] P.D. Barnes, Los Alamos Report No. LA-972-C, Vol. 1, 315 (1982).
- [10] A.T.M. Aerts and C.B. Dover, Phys. Rev. D **28**, 450 (1983).
- [11] M. Danysz *et al.*, Nucl. Phys. **49**, 121 (1963).
- [12] J. Prowse, Phys. Rev. Lett. **17**, 782 (1966). Considerable doubt persists on whether this event is a real double hypernucleus, since calculated yield is much less than one and no picture of the event was left.
- [13] C.B. Dover *et al.*, Phys. Rev. C **44**, 1905 (1991).
- [14] D. Zhu, C.B. Dover, A. Gal, and M. May, Phys. Rev. Lett. **67**, 2268 (1991).
- [15] M. Sano, M. Wakai, and Y. Yamamoto, Prog. Theor. Phys. **87**, 957 (1992).
- [16] T. Yamada and K. Ikeda, Phys. Rev. C **56**, 3216 (1997).

- [17] Y. Hirata, Y. Nara, A. Ohnishi, T. Harada, and J. Randrup, *Prog. Theor. Phys.* **102**, 89 (1999).
- [18] P. Khaustov *et al.*, *Phys. Rev. C* **61**, 027601 (2000).
- [19] J.K. Ahn *et al.*, *Phys. Lett. B* **378**, 53 (1996).
- [20] J.K. Ahn *et al.*, *Nucl. Phys.* **A648**, 263 (1999).
- [21] J.K. Ahn *et al.*, *Nucl. Phys.* **A625**, 231 (1997).
- [22] H. Toyokawa and M. Yosoi, RCNP-E81.
- [23] A. Ohnishi, Y. Hirata, Y. Nara, S. Shinmura, and Y. Akaishi, *Nucl. Phys.* **A670**, 297 (2000).
- [24] S. Aoki *et al.*, *Nucl. Phys.* **A644**, 365 (1998).
- [25] GEANT 3.21 - Detector Description and Simulation Tool, CERN Program Library, W5013 (1993).
- [26] G. Mechtersheimer *et al.*, *Phys. Lett.* **73B**, 115 (1978).
- [27] K. Imai *et al.* (unpublished); The ρ -stop/ σ -stop ratio obtained from E176 emulsion data was recalculated by requiring that σ -stop (n -prong events) should accompany track(s) longer than 0.4 mm.
- [28] C.J. Batty, *Nucl. Phys.* **A585**, 229c (1995).
- [29] M. Jurič *et al.*, *Nucl. Phys.* **B52**, 1 (1973). Binding energy of ${}_{\Lambda}^{12}\text{B}$ is quoted from this reference as $B_{\Lambda} = 11.37 \pm 0.06$ MeV.
- [30] Y. Yamamoto, M. Wakai, T. Motoba, and T. Fukuda, *Nucl. Phys.* **A625**, 107 (1997).
- [31] T. Motoba, H. Bandō, T. Fukuda, and J. Žofka, *Nucl. Phys.* **A534**, 597 (1991); T. Motoba, *ibid.* **A547**, 115c (1992); W. Gajewski *et al.*, *Nucl. Phys.* **B14**, 11 (1969).
- [32] U. Krecker, D. Kielczewska, and T. Tymieniecka, *Nucl. Phys.* **A236**, 491 (1974); A. Deloff, *ibid.* **A236**, 469 (1974).
- [33] K.S. Myint and Y. Akaishi, *Prog. Theor. Phys. Suppl.* **117**, 251 (1994).
- [34] M. May, *Nuovo Cimento A* **102**, 401 (1989).
- [35] J.F. Donoghue, E. Golowich, and B.R. Holstein, *Phys. Rev. D* **34**, 3434 (1986).
- [36] G.J. Feldman and R.D. Cousins, *Phys. Rev. D* **57**, 3873 (1998).
- [37] A.N. Alekseev *et al.*, *Yad. Fiz.* **52**, 1612 (1990) [*Sov. J. Nucl. Phys.* **52**, 1016 (1990)].
- [38] F. James, Monte Carlo Phase Space, CERN 68-15 (1968); GENBOD, N -body Monte Carlo Event Generator, CERN Program Library, W515.
- [39] J.K. Ahn *et al.*, *Nuovo Cimento A* **107**, 2415 (1994).
- [40] A. Alavi-Harati *et al.*, *Phys. Rev. Lett.* **84**, 2593 (2000).
- [41] J. Belz *et al.*, *Phys. Rev. Lett.* **76**, 3277 (1996). Addendum in J. Belz *et al.*, *Phys. Rev. C* **56**, 1164 (1997).